AIAA 94-0485

# Application of a Third Order Upwind Scheme to Viscous Flow over Clean and Iced Wings

A. Bangalore, N. Phaengsook and L. N. Sankar
School of Aerospace Engineering
Georgia Institute of Technology
Atlanta, GA

32nd Aerospace Sciences
Meeting & Exhibit
January 10-13, 1994 / Reno, NV

# APPLICATION OF A THIRD ORDER UPWIND SCHEME TO VISCOUS FLOW OVER CLEAN AND ICED WINGS

**A. Bangalore[1], N. Phaengsook[1] and L. N. Sankar[2]**
**School of Aerospace Engineering**
**Georgia Institute of Technology, Atlanta, GA 30332**

## ABSTRACT

A 3-D compressible Navier-Stokes solver has been developed and applied to 3-D viscous flow over clean and iced wings. This method uses a third order accurate finite volume scheme with flux difference splitting to model the inviscid fluxes, and second order accurate symmetric differences to model the viscous terms. The effects of turbulence are modeled using a k-ε model. In the vicinity of the solid walls, the k and ε values are modeled using Gorski's algebraic model. Sample results are presented for surface pressure distributions, for untapered swept clean and iced wings made of NACA 0012 airfoil sections. The leading edge of these sections are modified using a simulated ice shape. Comparisons with the experimental data obtained by Prof. Bragg at the University of Illinois are given.

## INTRODUCTION

The aerodynamic characteristics of lifting surfaces such as wings and horizontal tails may be dramatically altered by the accumulation of ice over the leading edge. Even a relatively small amount of ice accumulation may lead to dramatic rise in pressure drag, loss in lift, and in some cases, premature stall.

Under the support of the NASA Lewis Research Center, a research effort has been underway at Georgia Tech on the effects of icing on the aerodynamic performance of lifting surfaces. Both 2-D and 3-D analyses have been developed, and calibrated [Ref. 1-3]. These analyses used relatively simple algorithms to solve the compressible Navier-Stokes equations. For example, standard second order accurate central differences are used to model the derivatives in the governing equations. A fourth order low-pass filter is used at every time step for removing any high frequency spatial oscillations. These analyses also used simple algebraic turbulence models such as the Baldwin-Lomax model to account for the effects of turbulence. Finally, for the sake of computational stability and efficiency, these methods used an implicit time-marching algorithm that permit the use of very large time steps. Reliable convergence to steady state in less than 1 CPU hour of computer time on a Cray Y/MP class of computer, on a 100,000 point grid. Reasonable correlation was observed between the calculations and the measured data obtained by Bragg and his coworkers [Ref. 4].

As these analyses were applied to a number of iced wing calculations, two drawbacks of these approaches became apparent to the present investigators. First of all, the turbulence model used in these analyses is a simple algebraic eddy viscosity model, which uses the boundary layer thickness $\delta^*$ (or an equivalent quantity such as the distance from the wall, y) as the length scale of turbulent eddies. The algebraic model used the boundary layer edge velocity U(x) (or an equivalent quantity y $|\omega|_{max}$) as a measure of the velocity scale of turbulent eddies. Such a simple representation of turbulence works well only for simple attached or mildly separated flows. In the case of iced wings, the flow field contains boundary layer over the solid surfaces, reversed flow regions, and a free shear layer coming off sharp corners and turns associated with the ice shape. The turbulent length and velocity scales for free shear layers are clearly different from the wall bounded flows. Use of a simple eddy viscosity model to such complex flows lead to inaccurate results in regions of separation. For example, the length of the separation bubble was often inaccurately predicted. Potapczuk has discussed the limitations of the Baldwin-Lomax model, and has recommended phenomenological fixes to this model [Ref. 5].

The second drawback of the previous analyses is the irrecoverable filtering out and loss of information by the low-pass filters. These filters tend to smear out shock discontinuities, contact discontinuities, and shear layers. The rate at which the filtering is applied is proportional to $|u|+a$, where $|u|$ is the magnitude of local flow, and a is the speed of sound.

The present work improves upon the existing numerical analysis, presented in Ref. 3, and attempts to rectify the above two drawbacks. It uses a flux difference scheme, which dynamically and adaptively reduces the smearing of contact discontinuities, and vorticity waves, and leads to crisp resolution of free shear layers that arise in the flow [Ref. 6]. This method also uses a sophisticated

---

[1] Graduate Research Assistant
[2] Professor of Aerospace Engineering, Senior Member AIAA.

k-ε model to account for the effects of turbulence. In the vicinity of solid walls, this model uses a set of phenomenologically derived boundary conditions for k and ε, as described in Ref. 7. The improved analysis allows transition to be detected automatically by the solver as regions of very low turbulent kinetic energy.

The improved solver has been applied to clean and iced, swept wing configurations tested by Prof. Bragg and his coworkers at the University of Illinois, documented in the Ph. D. dissertation of Khodadoust [Ref. 8].

The rest of this paper is organized as follows. First, the Roe scheme is briefly outlined. Next, the k-ε formulation is described. Finally, several sample applications of the improved solver to iced wing analysis are presented

## MATHEMATICAL AND NUMERICAL FORMULATION

The 3-D compressible Navier-Stokes equations are given in a Cartesian coordinate system as

$$\frac{\partial q}{\partial t}+\frac{\partial F}{\partial x}+\frac{\partial G}{\partial y}+\frac{\partial H}{\partial z}=\frac{\partial R}{\partial x}+\frac{\partial S}{\partial y}+\frac{\partial T}{\partial z} \tag{1}$$

Here q is a vector of conserved flow properties; F, G and H are the inviscid flux vectors; R, S and T are viscous terms, which include the effects of turbulence through the eddy viscosity concept.

The calculations are carried out in a curvilinear body-fitted coordinate system (ξ,η,ζ). In this system, the governing equations may be written as

$$\frac{\partial \hat{q}}{\partial t}+\frac{\partial \hat{F}}{\partial \xi}+\frac{\partial \hat{G}}{\partial \eta}+\frac{\partial \hat{H}}{\partial \zeta}=\frac{\partial \hat{R}}{\partial \xi}+\frac{\partial \hat{S}}{\partial \eta}+\frac{\partial \hat{T}}{\partial \zeta} \tag{2}$$

where $\hat{q}$ etc. are related to their Cartesian counterparts by the metrics of transformation.

The Roe Scheme:

The objective of the time-marching algorithm is to advance the flow field at cells (or nodes (i,j,k) from a time level 'n' to the next time level 'n+1'. For this purpose, in the present work, equation (2) was discretized as follows:

$$\frac{\hat{q}^{n+1}_{i,j,k}-\hat{q}^{n}_{i,j,k}}{\Delta t}+\delta_\xi \bar{F}^{n+1}_{i,j,k}+\delta_\eta \bar{G}^{n+1}_{i,j,k}+\delta_\zeta \bar{H}^{n+1}_{i,j,k}=\delta_\xi \hat{R}^{n}_{i,j,k}+\delta_\eta \hat{S}^{n}_{i,j,k}+\delta_\zeta \hat{T}^{n}_{i,j,k} \tag{3}$$

where the operators $\delta_\xi$ etc. represent standard central differences such as

$$\delta_\xi \bar{F}=\frac{\bar{F}_{i+1/2}-\bar{F}_{i-1/2}}{\Delta\xi} \tag{4}$$

The numerical flux vector $\bar{F}$ differs from the physical flux vector $\hat{F}$ in a manner specified by Roe [Ref. 6]. Let $q_L$ and $q_R$ be two estimates to the flow field vector q, to the left side and right side of the cell face (i+1/2,j,k). Then,

$$\bar{F}_{i+1/2}=\frac{\hat{F}(q_L)+\hat{F}(q_R)}{2}+\frac{1}{2}T|\Lambda|T^{-1}(q_L-q_R)$$

*where*,

$$q_R=q_{i+1}-\frac{q_{i+1}-q_i}{3}-\frac{q_{i+2}-q_{i+1}}{6}$$

*and*

$$q_L=q_i+\frac{q_{i+1}-q_i}{3}+\frac{q_i-q_{i-1}}{6} \tag{5}$$

Here T is a matrix that contains the left eigenvectors of the matrix $\partial\hat{F}/\partial q$, and Λ contains the eigenvalues of this matrix. These quantities must be computed using special "Roe" averages of $q_L$ and $q_R$.

It may be shown that the above estimates of $q_L$ and $q_R$ lead to a spatially third order accurate formulation, on uniform grids and on mildly stretched grids.

Equation (3) represents a system of non-linear algebraic equations for the flow properties vector q at time level 'n+1'. Furthermore, each node (i,j+1,k) is coupled to its nine neighbors. Thus, this system of equations are highly coupled. The classical Beam-Warming approximate factorization scheme was used solve these coupled nonlinear equations, in a manner similar to that described in Reference 1.

K-ε Turbulence Model

The starting point is the Boussnesq assumption for the turbulent stresses.

$$-\rho\overline{u_i u_j}=\mu_t\left(\frac{\partial u_i}{\partial x_j}+\frac{\partial u_j}{\partial x_i}\right)-\frac{2}{3}\delta_{ij}\left(\mu_t\frac{\partial u_k}{\partial x_k}+\rho k\right)$$

The turbulent viscosity $\mu_t$ has to modeled. This is achieved by modeling two physically conceivable quantities, the turbulent kinetic energy k, and the dissipation rate $\varepsilon$. The basic high Reynolds number K-$\varepsilon$ model integrates the following transport equations for k and $\varepsilon$.

$$\rho\frac{Dk}{Dt} = \frac{\partial}{\partial X_i}\left(\frac{\mu_t}{\sigma_k}\right)\frac{\partial k}{\partial X_i} + P - \rho\varepsilon$$

$$\rho\frac{D\varepsilon}{Dt} = \frac{\partial}{\partial X_i}\left(\frac{\mu_t}{\sigma_\varepsilon}\right)\frac{\partial \varepsilon}{\partial X_i} + \frac{\varepsilon}{k}\left(C_1 P - C_2\rho\varepsilon\right)$$

The turbulent production $P_t$ is given by:

$$P = -\rho\overline{u_i u_j}\frac{\partial u_i}{\partial X_i}$$

and the turbulent viscosity $\mu_t$ is related to k and $\varepsilon$ by :

$$\mu_t = C_\mu\rho\frac{k^2}{\varepsilon}$$

The basic k-$\varepsilon$ model constants are as follows.

$$C_\mu = .09$$
$$C_1 = 1.43$$
$$C_2 = 1.92$$
$$\sigma_k = 1.0$$
$$\sigma_\varepsilon = 1.3$$

As in the case of the Navier-Stokes equations, the k-$\varepsilon$ equations were cast on a curvilinear coordinate system in conservation form, and solved using an ADI procedure. The source terms appearing in the k and $\varepsilon$ equations were lagged by one time step for simplicity. The turbulence model equations were solved separately at the end of every time step, after the mean flow properties had been computed. This resulted in the solution of a 2 x 2 system that may be efficiently solved.

The starting values for k and $\varepsilon$ were obtained assuming the flow to be in equilibrium. That is, the production and dissipation terms in the k-$\varepsilon$ equations were set to be equal. This results in a system of simultaneous *algebraic equations* for k and $\varepsilon$, which may be solved to initialize the turbulence field. These algebraic equations involve the eddy viscosity, which was computed using the Baldwin-Lomax model. Note that the Baldwin-Lomax model was used only at the start of the calculations to initialize the turbulence field, and is not needed during subsequent time steps.

Near solid walls, the classical high Reynolds number k-$\varepsilon$ model breaks down. In the present work, near the solid wall, the k and $\varepsilon$ were assumed to have the following variation:

$$k = A y^3$$

$$\varepsilon = \text{constant}$$

Herer the constant A was evaluted using the computed values of k sevral nodes away from the solid surface.

## RESULTS AND DISCUSSION

Navier-Stokes calculations were carried out using the flow solver developed in the previous section, for swept and unswept, untapered wing-alone geometries tested by Bragg et al. The airfoil sections are made of NACA 0012 airfoil sections. The wing tested had a chord length of 15 inches and a semispan of 37.25 inches. To study the effects of icing, the leading edge was modified with a simulated ice shape. This ice shape corresponds to that measured at the NASA Lewis Icing Research Tunnel. for a NACA 0012 airfoil, at a freestream velocity of 130 mph, angle of attack of 4 degrees, icing time of 4 minutes, volume median droplet diameter of 20 microns, liquid water content of 2.1 grams per cubic meter and a temperature of 18 degrees. Bragg's measurements were done at zero sweep and at a 30 degree sweep.

The calculations used a 121 x 24 x 45 grid, with 91 points on the airfoil at each span station, 14 spanwise stations over the wing, and 45 points in the direction normal to the wing surface. Roughly a quarter of these points are in the boundary layer region. Thus, the boundary layer is only moderately resolved in these preliminary calculations. Figure 1 shows the internally generated body-fitted grid used in the present simulations. Figure 2 shows a typical airfoil cross section, for the iced wing case.

Calculations have been carried for at least 16 of the possible 32 combinations: swept and unswept, clean and iced, angle of attack of 4 degrees and 8 degrees, Roe scheme and central difference scheme, Baldwin-Lomax model and k-$\varepsilon$ model. For the sake of brevity, only a small subset of the calculations carried out are discussed here in detail.

Figure 3 shows the surface pressure distribution for the clean wing at 8 degrees angle of attack at 3 spanwise locations, 42%, 56%, 72% and 89%. In these calculations, the Roe solver was used, and a Baldwin-Lomax model was employed. Because of the increased operations counts associated with the Roe scheme, the calculations were typically 30% more expensive per grid

point, per time step, compared to the original central difference scheme. The Roe solver was also stiff, requiring smaller time steps than the central difference scheme. Nevertheless, calculations similar to those shown on figure 3 could be obtained with the Roe/Baldwin-Lomax solver in about 1500 iterations, requiring about 90 minutes of CPU time on a Cray Y/MP system using a single processor.

Figure 4 shows the Roe/k-ε solver results for the same case. The results are comparable to the Baldwin-Lomax region, except near the leading edge region, where the Cp distribution shows a small plateau, indicative of a small amount of local separation. The k-ε model behaved well. The strong source terms cause the k-ε equation set to be stiff. These equations were therefore solved using a smaller (local) time step than the basic flow equations. Upper and lower limits were placed on the k and ε values, in order to prevent the solver from diverging at the start of the calculations. The flow solver had no other user adjustable constants, and was run using the standard k-ε constants described in the previous section. The final results for the k and ε fields were well within these upper and lower limits. Thus, these limits do not affect the quality of the final, converged solution. A typical k-ε solution required about 2 hours of CPU time, on a Cray Y/MP system, using a single processor. Work is now underway on reducing this time requirement.

Figure 5 shows the calculations and measurements for the swept iced wing at 4 degree angle of attack. In this case, the flow separates over the leading edge ice shape, and the pressure distribution forms a plateau. The Roe/k-ε solver is seen to perform satisfactorily at all the stations. It is seen that the plateau over the upper surface is well captured, while the plateau over the lower surface is not correctly captured. The solution downstream of the plateau region is in excellent agreement with the measurements.

Figure 6 shows some preliminary results for the velocity field at selected chordwise locations, for the iced swept wing. Both the k-ε results and the original algebraic model results are shown. The grid used in these two cases was identical. It appears that the k-ε model does a better job of predicting the velocity profile, both near the surface and near the boundary layer edge. The grid used in these two simulations was rather coarse in the normal direction. Additional calculations on finer grids are needed, before one can conclusively say which turbulence model is performing better. Nevertheless, the improved agreement with the k-ε model is encouraging.

## CONCLUDING REMARKS

An existing compressible Navier-Stokes solver for clean and iced wing analysis has been upgraded through the use of state of the art upwind difference schemes, and a two equation k-ε model. Encouraging results have been obtained for swept, clean and iced wing configurations. There is some additional overhead associated with the Roe scheme and the k-ε model. Work is needed on improvements to the algorithm to reduce the CPU time requirements. Additional systematic validation of the improved flow solver is now underway, prior to its adaptation for iced wing performance analysis.

## ACKNOWLEDGMENT

This work was supported by the NASA Lewis Research Center under Garnt NAG-3-768. Dr. Mark Potapczuk is the technical monitor.

## REFERENCES

1. Wu, Jiunn-Chi, "A Study of Unsteady Turbulent Flow past Airfoils," Ph. D. Dissertation, Georgia Institute of Technology, Atlanta, GA 1988.

2. Kwon, O. J., and Sankar, L. N., "Numerical Study of the Effects of Icing on Finite Wing Aerodynamics," AIAA Paper 90-0757.

3. Kwon, O. J. and Sankar, L. N., "Numerical Study of the Effects of Icing on Fixed and Rotary Wing Aerodynamics," AIAA paper 91-0662.

4. Bragg, M. B. and Khodadoust, A., "Effects of Simulated Glaze Ice on a Rectangular Wing," AIAA paper 89-0750.

5. Potapczuk, M., "Navier-Stokes Analysis of Airfoils with Leading Edge Ice Accretions," Ph. D. Dissertation, The University of Akron, Akron, Ohio, 1989.

6. Roe, P. L., "Approximate Riemann Solvers, Parameter Vectors and Difference Schemes," Journal of Computational Physics, Vol. 43, 1981, pp 357-372.

7. Gorski, J. J., "A New Near-Wall Formulation for the k-ε Equations of Turbulence," AIAA Paper 86-0556, 1986.

8. Khodadoust, A., "An Experimental Study of the Flow Field on a Semi-Span Wing with a Simulated Glaze Ice Accretion," Ph. D. Dissertation, University of Illinois at Urbana-Champaign, 1993.

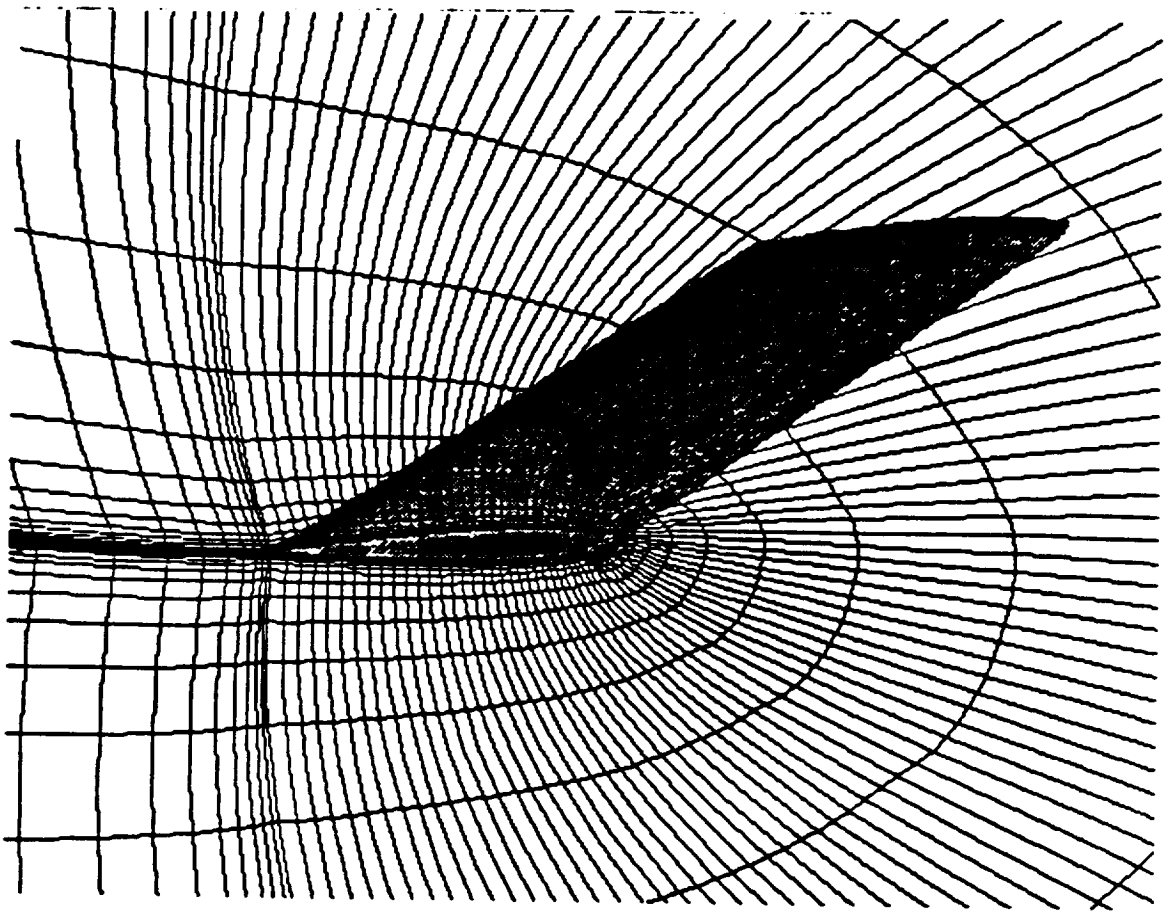

Fig : 1 Computational Grid (151X42X43) for iced wing with 30° sweep angle

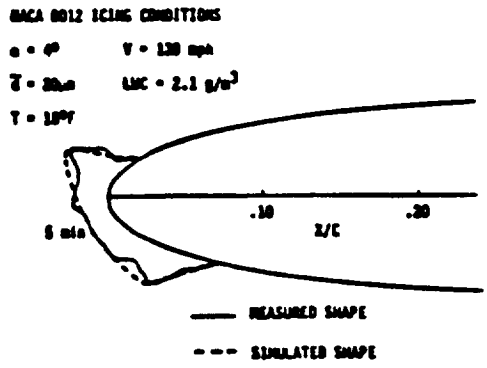


Fig 2 : Simulated Glaze ice accretion

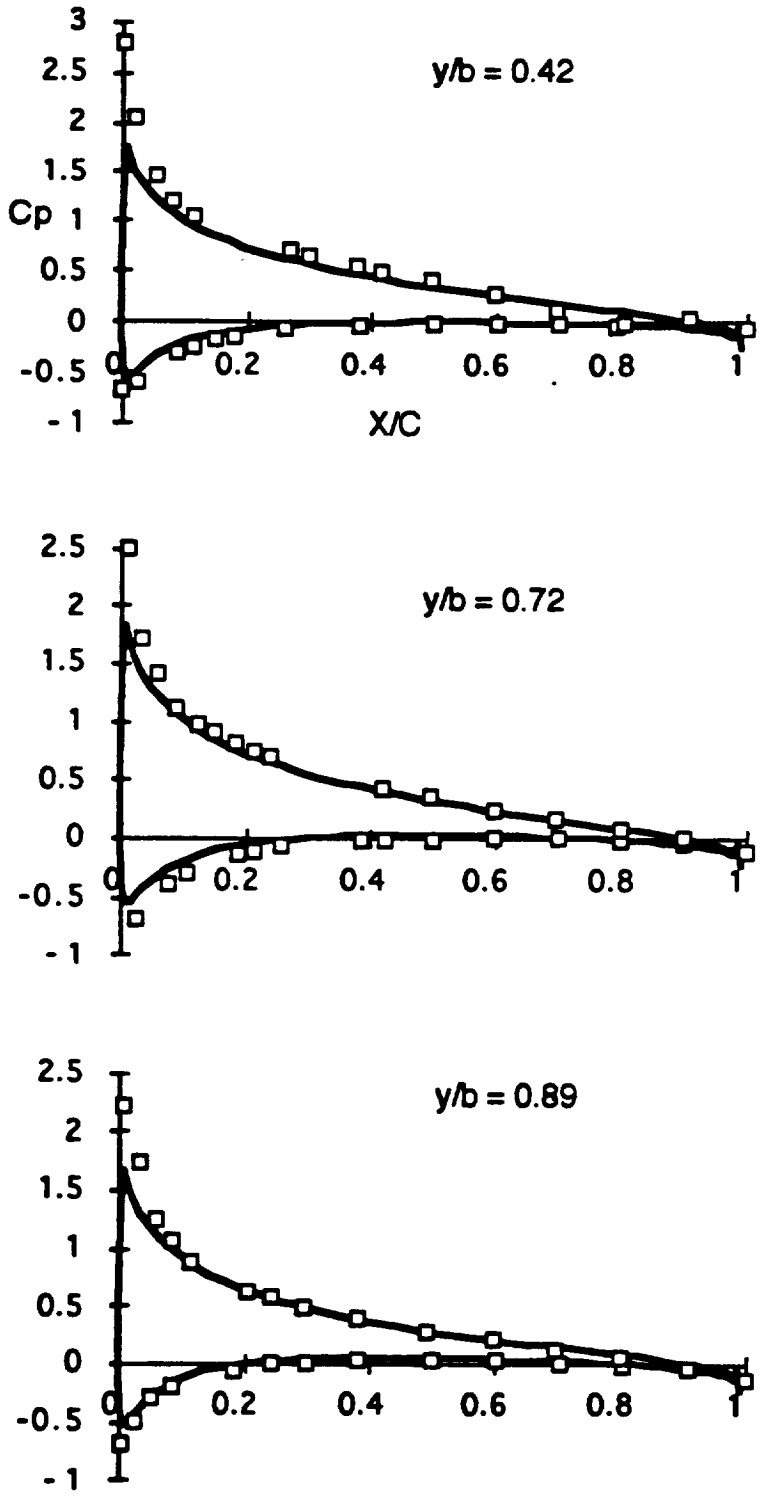


Figure 3. Surface pressure Distribution over a Clean Swept Wing at 8 Degree Angle of Attack, computed using Roe Scheme with Baldwin-Lomax Model, ____ Theory, □ Expt.

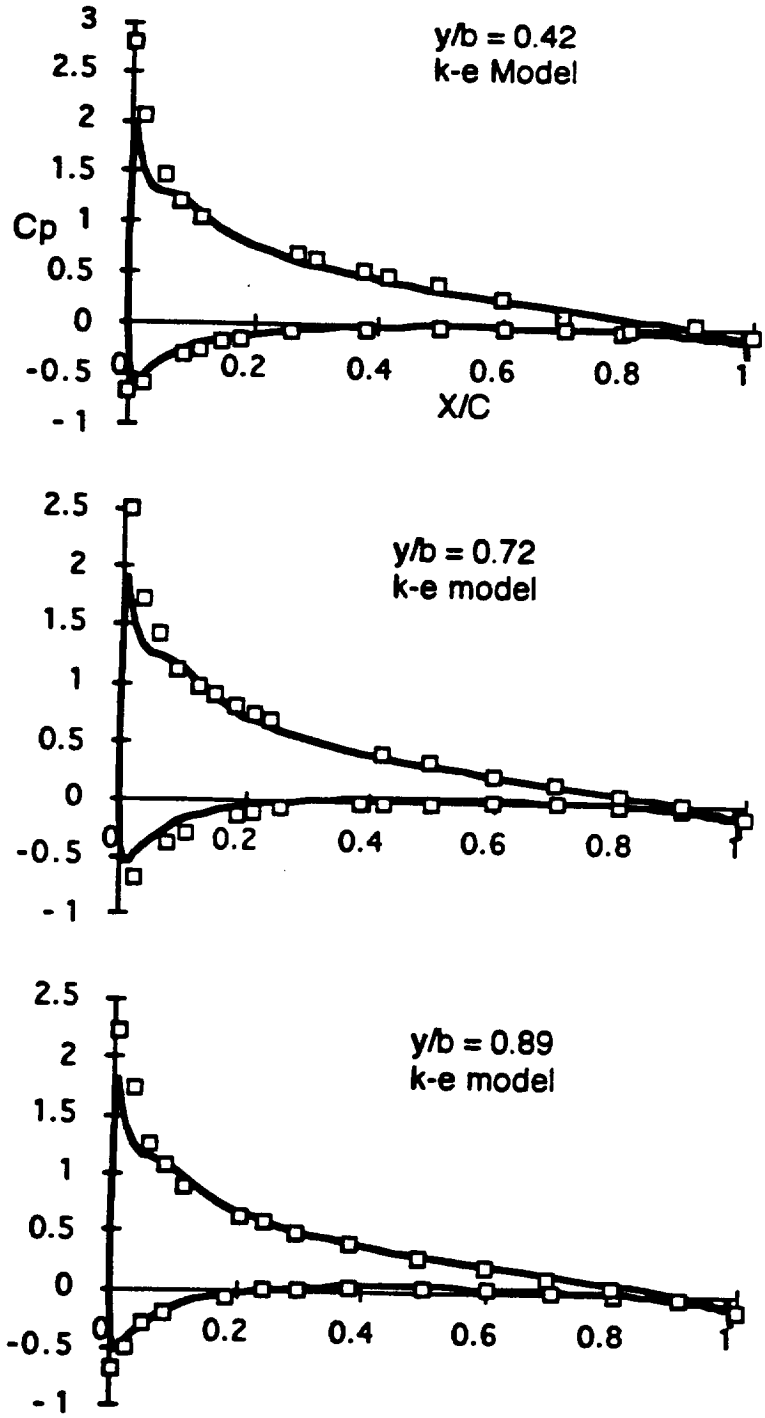


Figure 4. Surface Pressure Distribution over a clean Swept Wing using the Roe scheme and the k-ε turbulence model, ____ Theory, □ Expt

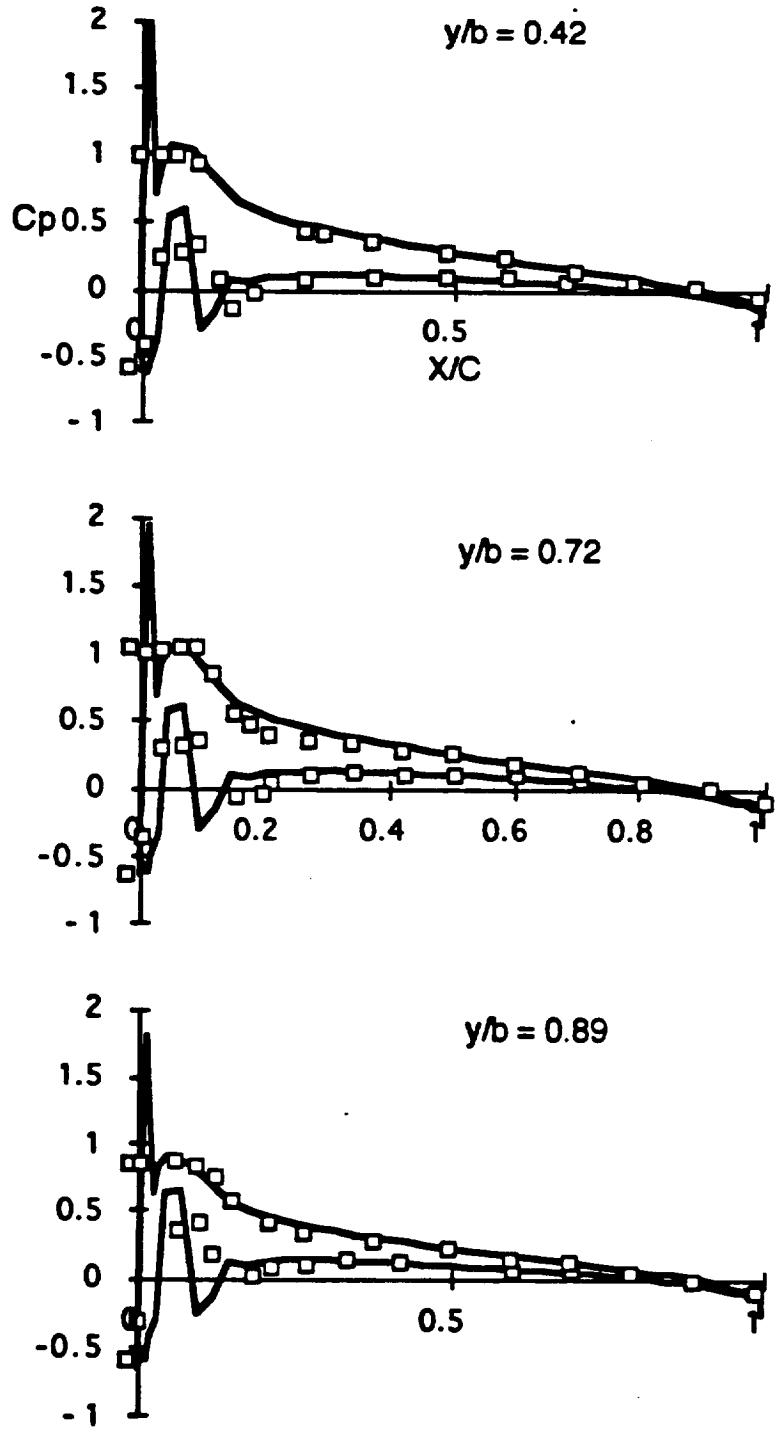


Figure 5. Surface Pressure Distribution over an Iced Swept Wing using the Roe scheme and the k-ε turbulence model, ____ Theory, □ Expt

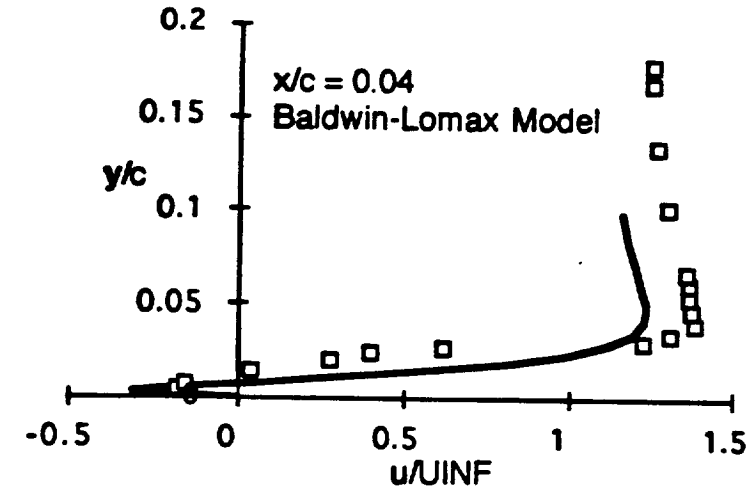


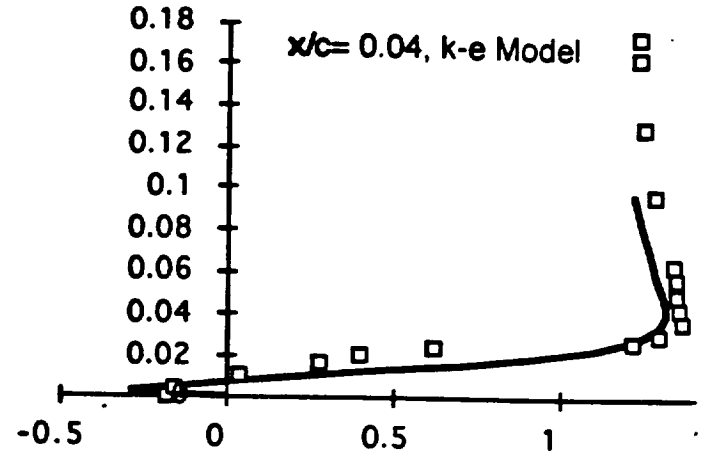


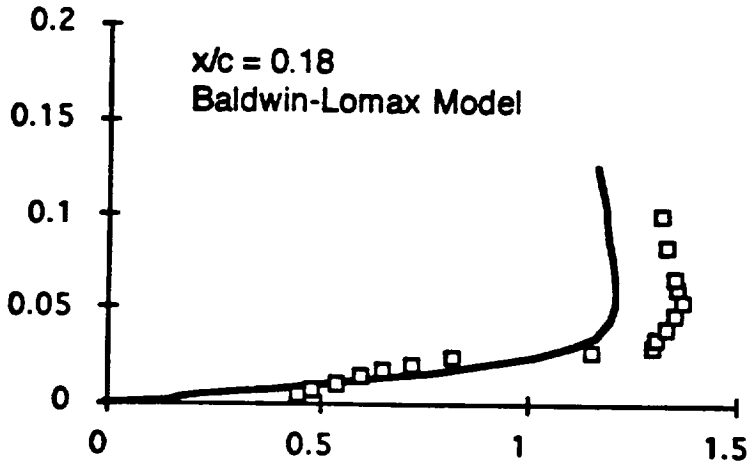


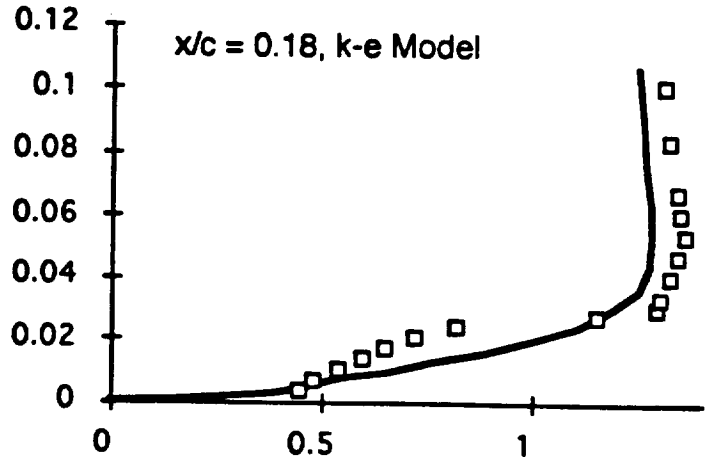


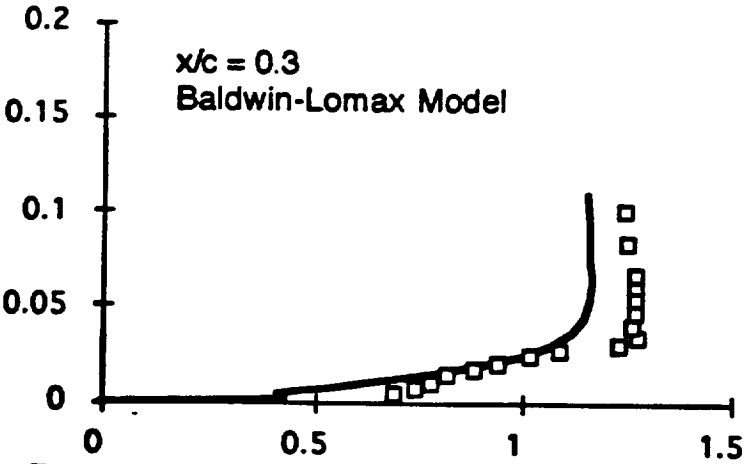


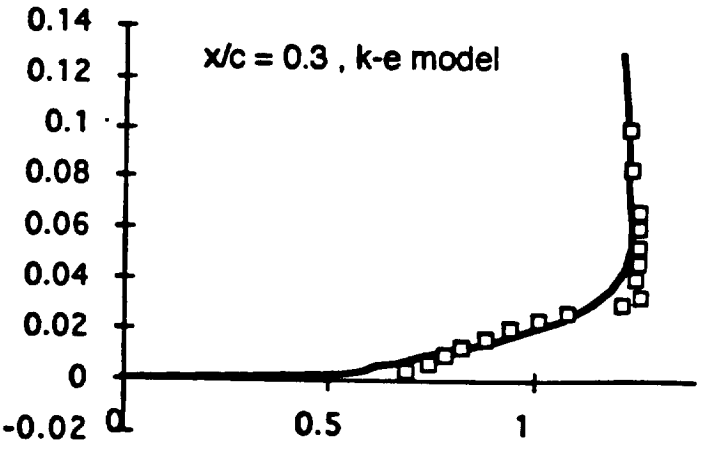


Figure 6. Velocity Profiles at a number of Stations for the Iced Swept Wing at 4 degrees Angle of Attack, ____ Theory, □ Expt